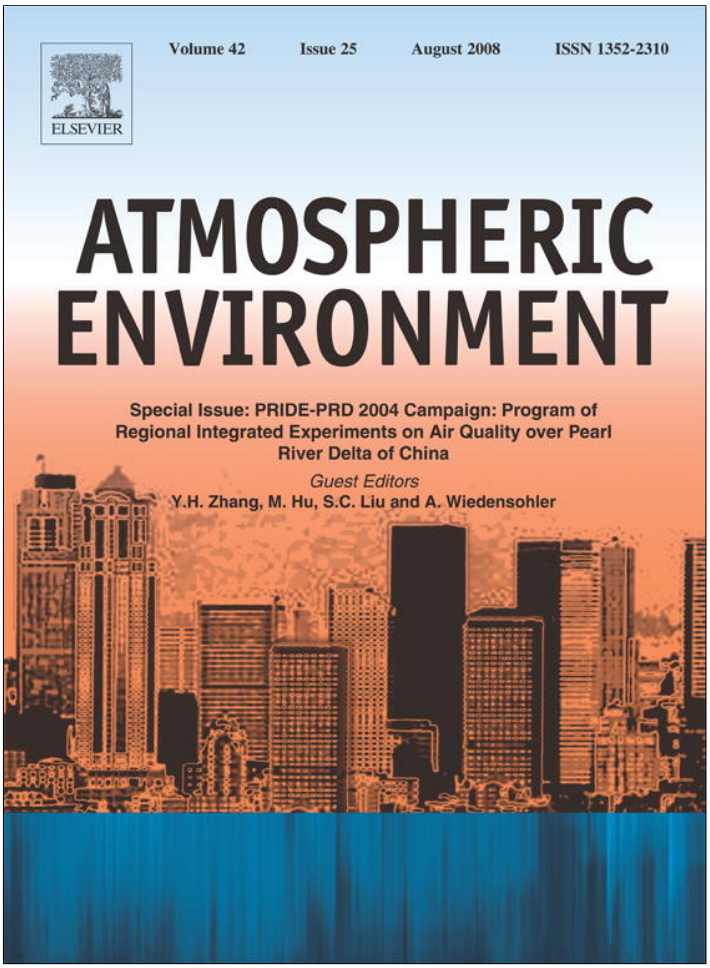

Available online at www.sciencedirect.com
ScienceDirect
Atmospheric Environment 42 (2008) 6321–6334
ATMOSPHERIC ENVIRONMENT
www.elsevier.com/locate/atmosenv

Hygroscopic properties and extinction of aerosol particles at ambient relative humidity in South-Eastern China

H. Eichler[a,c,*], Y.F. Cheng[a,b], W. Birmili[a], A. Nowak[a], A. Wiedensohler[a], E. Brüggemann[a], T. Gnauk[a], H. Herrmann[a], D. Althausen[a], A. Ansmann[a], R. Engelmann[a], M. Tesche[a], M. Wendisch[c], Y.H. Zhang[b], M. Hu[b], S. Liu[b], L.M. Zeng[b]

[a]*Leibniz-Institute for Tropospheric Research (IfT), Permoserstr. 15, 04318 Leipzig, Germany*
[b]*College of Environmental Sciences, Peking University, 100871 Beijing, China*
[c]*Institute for Atmospheric Physics, Johannes Gutenberg University Mainz, 55009 Mainz, Germany*

Received 31 August 2007; received in revised form 23 May 2008; accepted 29 May 2008

Abstract

During the "Program of Regional Integrated Experiments of Air Quality over Pearl River Delta 2004 (PRIDE-PRD2004)" hygroscopic properties of particles in the diameter range 22 nm to 10 μm were determined. For that purpose, a Humidifying Differential Mobility Particle Sizer (H-DMPS) and a Micro-Orifice Uniform Deposition Impactor (MOUDI) were operated. The derived size-dependent particle hygroscopic growth factors were interpolated to ambient relative humidity (RH) and used to calculate the particle number size distributions (PNSDs) at ambient conditions. A comparison between the modeled particle extinction coefficients ($\sigma_{ext,Mie}$) and those observed with a Raman lidar was made. It is shown that the particle extinction coefficient (σ_{ext}) at ambient RH can be properly estimated with Mie-model calculations based on the in situ physico-chemical measurements of dry and humidified PNSD and chemical composition.

Keywords: Hygroscopicity; Descriptive hygroscopic growth factor; H-DMPS; PRD; Particle extinction coefficient

1. Introduction

Aerosol particles cause direct climate effects by scattering and absorbing solar radiation (e.g., Anderson et al., 2003; IPCC, 2007). The impact of aerosol particles on the solar radiation budget is presumably negative but large uncertainties on the amount of the cooling still exist. Furthermore, the light absorption effect of the particles leads to a warming of the aerosol layers. In order to decrease the uncertainties of the radiative effects of atmospheric aerosol particles in global climate models, physical and chemical properties of the aerosol particles, which in turn influence their optical properties, have to be characterized. In this context, an important particle property is the hygroscopicity. The hygroscopic properties of atmospheric aerosol particles influence ambient particle size, density and mass which in turn control the life time and removal mechanisms of the particles. Also, the aqueous-phase chemistry depends on the amount of

*Corresponding author.
E-mail address: eichlerH@uni-mainz.de (H. Eichler).

1352-2310/$ - see front matter © 2008 Elsevier Ltd. All rights reserved.
doi:10.1016/j.atmosenv.2008.05.007

condensed water as already reported by Hänel (1976) and Winkler (1988). Condensation of water changes the particles' light scattering properties by changing the particle size and refractive index (Covert et al., 1972). Finally, the particle size and the amount of hygroscopic material contained in the particles determine if they can act as cloud condensation nuclei (CCN) or remain as interstitial aerosol particles at supersaturations typical in clouds (Heintzenberg and Covert, 1990). Moreover, the hygroscopic growth of aerosol particles has an influence on atmospheric visibility (Tang, 1981).

Investigations in South-Eastern China are of particular interest because of the rapidly proceeding industrialization which leads to a strong increase in emissions of anthropogenic particles. There is a need to characterize these aerosol particles to determine their influence on climate. Characterization of the aerosol particle properties was therefore one of the aims of the project PRIDE-PRD2004, for a more detailed description of the scientific goals see Cheng et al. (2006). As mentioned above, hygroscopicity is an important parameter and was therefore measured during the field experiment in the Pearl River Delta (PRD) in fall 2004. The Humidifying Differential Mobility Particle Sizer (H-DMPS) was used to measure particle number size distributions (PNSDs) of 22–900 nm sized aerosol particles at pre-defined relative humidities between 30% and 91% with a time resolution of roughly 15 min (Nowak, 2005). By using a Twin Differential Mobility Particle Sizer (TDMPS) and a H-DMPS in parallel and having additional data of the chemical composition of the particles from a Micro-Orifice Uniform Deposition Impactor (MOUDI, size range: 0.1–18 μm), hygroscopic particle growth factors as functions of particle size were determined. These were used to calculate the PNSD at ambient relative humidity (RH). By knowledge of this ambient PNSD and the chemical composition of the particles, the optical properties, e.g., the particle light extinction coefficient were derived from Mie theory.

2. Experimental

2.1. Field experiment

The dataset this study is based on was collected at the rural background site Xinken (22.6°N, 113.6°E) during 4 October–5 November 2004. The measurement site was situated at a branch of the Pearl River on the western edge of the river delta. See Cheng et al. (2006) or Zhang et al. (2008) for a detailed description of the experimental setup. Except for the MOUDI, the instruments used to characterize the hygroscopic growth properties were placed inside a laboratory container. In addition to the instruments described below, the container was equipped with a three-wavelength integrating nephelometer (TSI 3563) and a MAAP (Multi-Angle Absorption Photometer, Thermo 5012) to determine the optical properties of the dry aerosol population. An air-conditioner ensured stable temperatures inside the container, which are crucial for the performance of the H-DMPS.

2.2. Particle number size distributions (PNSDs)

2.2.1. Measurements of dry PNSD

The PNSD of dry particles was measured with a TDMPS (Birmili and Wiedensohler, 1997) covering the size range 3–900 nm (electrical mobility diameter). Furthermore, an Aerodynamic Particle Sizer (APS, TSI Model 3320, size range: 0.8–10 μm aerodynamic diameter) was used to extend the size range of the dry PNSD measurement. The time resolution of the TDMPS was 15 min, the one of the APS was 5 min. PNSD measurements from both instruments were made from 4 October to 5 November 2004 (Day of Year, DOY, 278–310). Upstream of the TDMPS and the HDMPS driers based on Nafion membrane technology were installed to decrease the RH in the aerosol sampling line to below 10%. The sheath air needed for the TDMPS and H-DMPS was supplied by a compressor and dried after entering the measurement container using an adsorption drier.

2.2.2. Measurements of humidified PNSD

During 16 October–5 November (DOY 290–310) PNSDs for 22–900 nm particles at defined RHs were measured with a H-DMPS (Nowak, 2005). The measurement principle is similar to the TDMPS except that the H-DMPS measures humidified PNSD at controlled RH. The setup of the H-DMPS is shown in Fig. 1.

During the PRD experiment, the H-DMPS was operated at RH of 30%, 57%, 78% and 91%. Humidity and temperature sensors (HMP230, Vaisala Inc., Helsinki, Finland) and differential pressure transducers were used to continuously monitor RH, temperature and flows inside the H-DMPS. The humidity sensors were calibrated

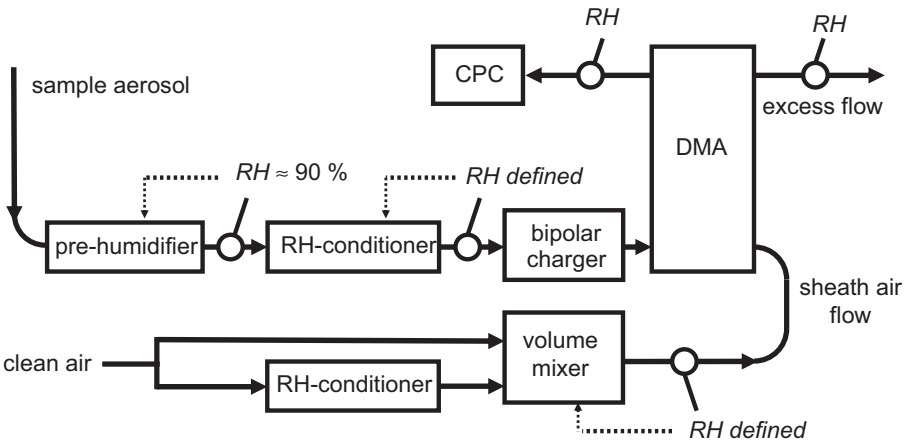

Fig. 1. Setup of the Humidifying Differential Mobility Particle Sizer (H-DMPS). DMA: Differential Mobility Analyzer. CPC: Condensation Particle Counter. Feedback regulations are indicated by dotted lines.

with a dew point mirror prior to the field experiment. Upstream of the H-DMPS, the sample aerosol flow of 0.5 lpm (liters per minute) was humidified to approximately 90% RH in a diffusion humidifier (ANSYCO Inc., Karlsruhe, Germany, Model MH-110-12S) to ensure that the sample aerosol originates from a state above the known deliquescence point of inorganic salts being relevant in the atmosphere. Because of that pre-humidification to 90% RH, one can assume that hygroscopic particles or particles consisting of mixtures of hygroscopic and hydrophobic compounds such as mineral dust or crystalline organics are spherical solution droplets as shown in Sjogren et al. (2007). Entirely hydrophobic particles though will not form spherical solution droplets. The pre-humidifier is followed by the RH-conditioner in which the aerosol flow is brought to the desired RH inside a membrane gas diffusion drier (MD-drier, ANSYCO Inc., Model MD-110-12F). With a DMA (Differential Mobility Analyzer, Vienna-type, center rod length 28 cm; Winkelmayr, 1991), particles were selected according to their electrical mobility. Before the aerosol flow entered the DMA, it passed through a bipolar Kr-85 charger in which the particles were charge-neutralized at the target RH. As shown in Fig. 1, an RH-conditioning procedure is also applied to the sheath air (5 lpm) before being injected into the DMA. Downstream of the DMA, monodisperse particles are counted with a Condensation Particle Counter (CPC, TSI 3010). One complete H-DMPS scan (22–900 nm) took about 13 min. At each RH, three scans are logged before the dry and wet flows get mixed differently to adjust to a new RH. One complete cycle over all four RHs is completed within about 3.5–4 h. Using a TDMPS and a H-DMPS in parallel allows to measure dry and humidified PNSD simultaneously. This approach also enables to calculate size-resolved hygroscopic growth factors. The residence times of the particles in the pre-humidifier and the sampling line from the pre-humidifier to the DMA are about 1.5 and 25 s, respectively. In recent studies, attention has been raised to the question of required residence times at the specified humidity to ensure equilibrium after water uptake (Chan and Chan, 2005; Sjogren et al., 2007). While inorganic salts have water vapor equilibration times of less than 1 s it was lately found that some inorganic/organic mixed-phase solutions required residence times of >40 s to reach equilibrium (Sjogren et al., 2007). However, Chuang (2003) reported that during the dry and wet season in Mexico City only a small fraction of particles exhibited equilibrium times between 3 and 33 s while most atmospheric particles reached their equilibrium sizes in 2–3 s. In practice, having two opposing requirements in mind, a compromise between long residence times (requiring long conditioning lines) and little diffusion losses (requiring short conditioning lines) had to be found when constructing the H-DMPS.

2.3. Chemical composition and mass size distribution

During 1 week of the campaign (23–30 October, DOY 297–304), the mass size distribution and the chemical composition of aerosol particles in PRD were measured with a 10-stage MOUDI (Model MSP 110, 50% aerodynamic cut-off diameters: 0.1/0.18/0.32/0.56/1.0/1.8/3.2/5.6/10.0/18.0 μm).

The MOUDI was operated at ambient conditions with a time resolution of 12 h. Daytime measurements were made from 8:00 to 20:00; nighttime measurements from 20:00 to 8:00 the following day. In total, 16 MOUDI samples were taken.

The mass concentration of the particles on the impactor samples was determined gravimetrically after conditioning the samples at 20 °C and a constant RH of 52%. A carbon analyzer C-mat 5500 (manufactured by Ströhlein) was used to analyze the elemental carbon (EC) and organic carbon (OC) mass concentration. The mass concentration of anions (Cl^-, NO_3^-, SO_4^{2-}) was measured with capillary zone electrophoresis using a Spectra Phoresis instrument (Thermo Separation Products, USA) while cations ($NH_4^+, Na^+, K^+, Mg^{2+}, Ca^{2+}$) were determined with ion chromatography (Metron, Switzerland). Since ion-mass concentrations on the impactor stages 1, 2 and 10 were very small or even below the detection limit of the ion-analysis instruments, the hygroscopic growth factor from chemical measurements could only be determined for the impactor stages 3–9 corresponding to aerodynamic particles sizes in the range of 100 nm–5.6 μm. A detailed description of the chemical analysis of the MOUDI samples is given in Liu et al. (2008) and Gnauk et al. (2008).

3. Data processing

3.1. Data handling and quality control

The particle mobility distributions measured by the TDMPS and H-DMPS were inverted using an algorithm developed by Stratmann and Wiedensohler (1996). By considering multiply charged particles, the size-dependent DMA transfer function and the counting efficiency of the CPCs it calculates the PNSD ($dN/d\log D_p$) as number of particles per cm^3. Particle-size-dependent tubing losses due to particle diffusion and gravitational settling were assessed according to Willeke and Baron (1993).

After averaging the APS data over 15 min, the aerodynamic particle diameter $D_{p_{aero}}$ measured with the APS was converted to Stokes-equivalent diameter D_p by dividing $D_{p_{aero}}$ with the square root of the assumed density of the dry aerosol particles of 1.7 g cm^{-3} (Cheng et al., 2006). Then, the APS and TDMPS data were combined to get a composite dry PNSD in the range 3 nm–10 μm.

Quality criteria for the TDMPS and H-DMPS data were defined after the field campaign to assure an accurate determination of the descriptive hygroscopic growth factors (DGF). Only humidified PNSD fulfilling the following criteria were used for further analysis:

- RH of the pre-humidifier >82%,
- <2% aerosol and sheath air flow deviation from target value,
- <0.5 K temperature gradient in the DMA for scans at 30%, 57% and 78% RH,
- <0.25 K temperature gradient in the DMA for scans at 91% RH.

The flow rates of the TDMPS and H-DMPS were regulated automatically with mass flow controllers. Flow rates of the TDMPS, H-DMPS and APS were checked once a week with a commercial bubble flow meter having an accuracy of ±1%. Therefore an allowed flow variation of 2% was reasonable. For dry PNSD, the stability of the flows was considered as quality assurance criteria. The allowed temperature gradients of 0.5 and 0.25 K result in an uncertainty of RH of 3% or 1.5%, respectively. At 91% RH a more rigorous criteria for the temperature gradient was chosen because the sensitivity of hygroscopic growth factor on RH increases with increasing RH.

In order to calculate hygroscopic growth factors from dry and wet PNSD, TDMPS scans were matched to corresponding H-DMPS scans with an allowed time-lag of 3 min between the two data sets.

An important premise for calculating the descriptive hygroscopic growth factor DGF is that the total number concentrations of TDMPS and H-DMPS are equal. This precondition was often not met. Observed ratios R of the total number concentration of H-DMPS to TDMPS varied between 0.4 and 1.8, with an average of 1.12. Because of the number concentration measurement uncertainty of both instruments of 10%, data with R outside of the 0.8–1.2 range was discarded. To realize the premise of equal total number concentrations of H-DMPS and TDMPS, the TDMPS data were scaled.

3.2. Descriptive hygroscopic growth factor (DGF)

The summation method introduced by Birmili et al. (2004) was used to determine DGF as a function of particle size by relating the two data sets of dry and humidified PNSD, measured in parallel with TDMPS and H-DMPS, respectively. If the assumption of equal total number concentrations of

particles in both size spectrometers is appropriate, each particle under the dry PNSD has a corresponding particle under the humidified PNSD. In practice, each PNSD was divided into 500 number concentration segments, each segment corresponding to $\frac{1}{500}$ of the total number of a distribution. By dividing the mean diameter of a "wet" segment by the mean diameter of its corresponding "dry" segment, a growth factor can be determined as a function of dry particle size: $\mathrm{DGF} = D_{p_{wet}}/D_{p_{dry}}$. As a result, a descriptive hygroscopic growth factor curve $\mathrm{DGF}(D_{p_{dry}})$ having 500 data points was obtained for each pair of concurrently measured dry/humidified PNSD.

The summation method is a statistical method relating dry and humidified PNSDs. In a statistical approach, it is assumed that all particles of a certain dry diameter grow to a certain wet size during humidification. However, we are aware that when measured close to sources, aerosol populations can also be externally mixed in chemical composition resulting in different hygroscopic properties of same-sized particles. Consequently, the DGFs are only indicative of the mean hygroscopic growth factors averaged over a monodisperse dry particle population. As the main purpose of the summation method is to provide a numerical tool to relate dry and humidified PSNDs, this limitation is not critical to the application of the DGFs. An outcome of this work was that the DGFs calculated using the summation method appeared to be a function of chemical particle composition; therefore DGFs were calculated and averaged over distinct time periods representative of different air masses observed during the field campaign.

Using the summation method, DGFs were calculated for the four RHs of the H-DMPS (30%, 57%, 78%, 91%). The DGFs of the defined RHs were then used in the empirical function (Eq. (1)) to determine the size-dependent fit-parameter a. The hygroscopic growth law (Eq. (1)) was then used to calculate the DGF at ambient RH:

$$\mathrm{DGF(RH)} = 1 + \frac{a}{1 - 0.01 \cdot \mathrm{RH}} \quad (1)$$

The dependence of the DGF for dry particles with diameters of 80, 140 and 380 nm on RH is shown in Fig. 2. The uncertainty ranges reflect the potential for error at the 99% confidence level (three standard deviations). The size dependence of the DGF is illustrated, particles in the Aitken mode (80 nm dry size) exhibit less hygroscopic growth than accumulation mode particles (140 and 380 nm). As stated in Birmili et al. (2008), the increase of DGF with increasing particle size could be attributed to cloud activation during which soluble material is added to the particles.

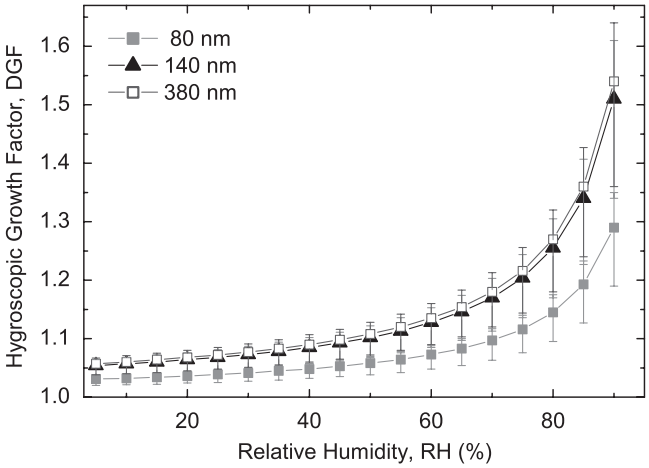

Fig. 2. Dependence of the DGF on relative humidity for selected dry particle sizes.

3.3. Growth factor calculation from MOUDI data (MGF)

Hygroscopic growth factors were also determined from the analyzed ion-mass concentrations on each impactor stage. Knowing the volume fractions and the hygroscopic growth behavior of each soluble constituent (i.e., of the individual inorganic salts) the hygroscopic growth factors of the particles on each impactor stage can be estimated using the subsequently described model.

In the first step, the combinations of anions and cations to molecules of inorganic salts on each impactor stage were estimated. The mass concentrations of the ions were converted to moles and, via stoichiometrical calculations, the amounts of the formed inorganic salts were determined. The major ionic constituents SO_4^{2-}, NH_4^+ and NO_3^- add up to about 20–70% of the dry mass concentration of the particles. The salts NH_4NO_3, $(NH_4)_2SO_4$ and NH_4HSO_4 are composed of these major ions and were therefore included in the model. At impactor stages 3 and 4 (1.8–5.6 μm), the amounts of sodium, chloride and calcium were significant. Consequently, reactions to NaCl, $NaNO_3$, $Ca(NO_3)_2$, Na_2SO_4, $NaHSO_4$ and $CaSO_4$ were modeled. Moreover, KNO_3 and sulfuric acid H_2SO_4 were considered in the model.

No detailed chemical analysis of organic compounds was made. For that reason, the hygroscopic growth factor of organics was considered to be unity in a first estimation of MGF. As stated in the review papers of organic aerosols by Saxena and Hildemann (1996) and Kanakidou et al. (2005) as well as in Dinar et al. (2007), the hygroscopic growth behavior of particulate organic mass (POM) depends on the source and residence time in the atmosphere due to the associated influence of physical and chemical ageing processes. Recent laboratory studies deal with the hygroscopic behavior of mixed particles containing inorganic and organic compounds (Zardini et al., 2008).

In order to estimate the influence of taking hygroscopic growth of POM into account in the determination of MGF, a scenario study was made: as a rough estimate, 50% of the sub-micron undefined mass fraction was attributed to POM (Cheng et al., 2008). Of that fraction, 50% was assumed to be water soluble organic compounds (WSOC) which is thought to be a reasonable estimate in accordance with reported WSOC fractions of 10–50% in Asia (Mader et al., 2004). At 91% RH, the sub-micron organic fraction was estimated to have growth factor of 1.2. This growth factor was chosen according to Peng et al. (2001), taking into account that Gnauk et al. (2008) identified oxalate, malonate and succinate in the impactor samples. For super-micron particles the POM hygroscopic growth was considered to be unity because only a very small fraction of the undefined mass could be apportioned to POM. At impactor stages 7–9 (100–560 nm) though, the mass fraction of POM amounted to 16–33% of the total dry mass.

In the second step, the hygroscopic growth factors of the individual inorganic salts i were determined with modified Köhler theory according to Tang (1996). For RHs below the crystallization RH (CRH) of the salts the growth factors equal unity.

In the third step, following Eq. (2), the water volume (V_{water}) on each impactor stage was calculated based on the hygroscopic growth factors GF_i of the salt i valid at 52% RH where the mass of the filters was determined:

$$V_{water} = \sum_{i=1}^{N} V_i \cdot GF_i^3 - V_i \quad (2)$$

N is the number of salts used in the model. The densities needed to convert the mass concentrations of the salts to volume concentrations V_i are listed in Table 1.

To calculate the volume fraction ε_i of each salt, the *dry* mass concentrations were determined by subtracting the water mass being present on the filters at 52% RH from the weighed mass. Mass concentrations of the dry particles were converted to volume concentrations (V_{dry}). Also, the insoluble volume (V_{insol}) was calculated as difference between the sum of the volume concentrations of the salts and V_{dry}. The volume fraction ε_i of each salt and of the insoluble volume then is the ratio of V_i to V_{dry}.

Finally, with the assumption of internally mixed particles, the hygroscopic growth factor MGF of each impactor size range at ambient RH was determined according to Eq. (3). The hygroscopic growth factor of the insoluble volume fraction ε_{insol} is unity at every RH:

$$MGF(RH) = \left[\sum_{i=1}^{N} \varepsilon_i \cdot (GF_i(RH))^3\right]^{1/3} \quad (3)$$

The particles were collected according to their aerodynamic particle size at ambient RH. Consequently, the aerodynamic size ranges of the impactor stages had to be converted to dry Stokes D_p according to Eqs. (4) and (5) to allow comparisons and an extrapolation between the growth factors determined from chemical analysis (MGF) and the descriptive hygroscopic growth factor (DGF) as demonstrated in Fig. 3:

$$\rho_{p_{wet}} = \frac{V_{dry}}{V_{dry} + V_{water}} \rho_{p,dry} + \frac{V_{water}}{V_{dry} + V_{water}} \rho_{water} \quad (4)$$

Table 1
Densities of inorganic salts and H_2SO_4 as well as corresponding recrystallization and deliquescence relative humidities CRH and DRH

Salt	Density ($g\,cm^{-3}$)	CRH (%)	DRH (%)
NaCl	2.165	46	75.3
$NaNO_3$	2.261	30	74.5
NH_4NO_3	1.725	25	62
NH_4HSO_4	1.78	20	40
$(NH_4)_2SO_4$	1.76	37	80
Na_2SO_4	2.68	59	84
$NaHSO_4$	2.476	<0.05	52
H_2SO_4	1.84	Liquid at room temperature	

Densities, DRH and CRH taken from Tang (1996), Tang and Munkelwitz (1994) and Johnson et al. (2004).

$$D_{p_{Stokes,dry}} = \frac{D_{p_{aero,wet}}}{\sqrt{\rho_{wet}}} \frac{1}{MGF} \quad (5)$$

3.4. DGF–MGF combination and uncertainty

The growth factors obtained from the two presented methods were compared. Presented here (Fig. 3) are the DGF and MGF at 91% RH for three days. Similar results were obtained for the other days. In the overlap region of the DGF and the MGF the mean percentage deviation of the growth factors at high RHs (91% RH) was roughly 1–8% as illustrated also in Table 2. In order to apply hygroscopic growth properties to the entire size range (22 nm–10 μm), the DGF and MGF were combined and extrapolated as presented in Fig. 3. For particle diameters below 300 nm the DGFs were used as input for the extrapolation while for bigger particles the MGF derived from MOUDI data were taken.

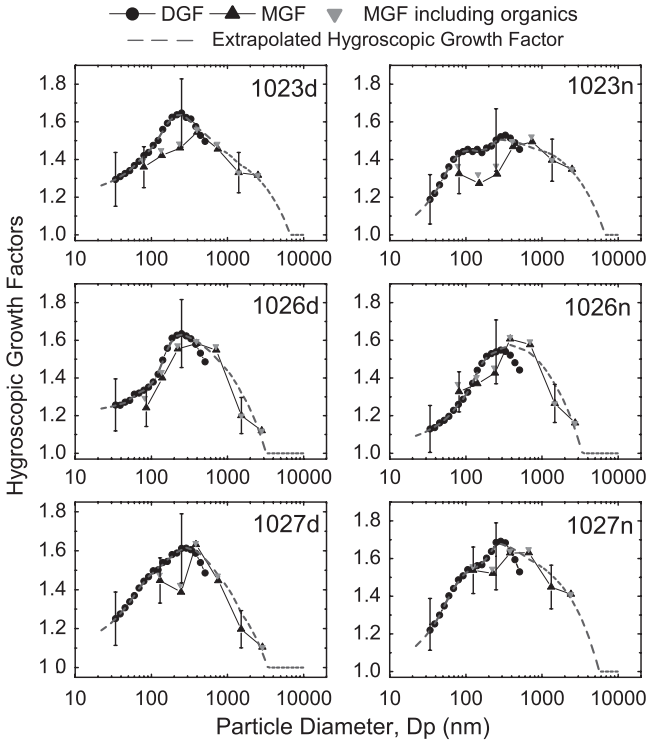

Fig. 3. Extrapolation of the growth factors at 91% RH. Black circles represent the DGF determined from H-DMPS data. Black triangles mark the MGF calculated from MOUDI data assuming the growth factor of organics equals unity, while gray triangles refer to the MGF including hygroscopic growth of organics. The dashed gray line shows the result of the extrapolation. "d" and "n" refer to daytime and nighttime measurements, respectively. The date is indicated by month and day, e.g., "1023". Error bars represent one standard deviation.

For particles smaller than 380 nm, MGFs are generally smaller than DGFs. Including the hygroscopic growth of organics results in an increase of MGF by about 1–3% on average for particle diameters of 80–250 nm. From the scenario study it can be concluded that taking into account the estimated hygroscopic growth of POM leads to an increase in MGF and thereby reduces differences between MGF and DGF. However, it cannot fully explain the observed differences. Another aspect is that the ion-equivalent balance did not equal zero. Especially in the size range 320–560 nm the negative inorganic ions turned out to be more abundant. It may be possible that not all ion species were detected and therefore some inorganic salts could not be included in the hygroscopic growth model. Furthermore, the ion-equivalent imbalance might be due to measurement uncertainties of the ion chromatography analysis and the capillary zone electrophoresis.

The influence of uncertainties in measurement and data analysis procedures on DGF and MGF was checked. A potential for uncertainties of DGF lies in the uncertainties of the RH sensors. The allowed temperature gradients of 0.5 K during scans of pre-defined RH of 30–78% and of 0.25 K at 91% RH result in an uncertainty of 3% RH and 1.5%

Table 2
Mean hygroscopic growth factors at 91% RH and percentage deviations of the DGF, the MGF assuming the growth factor of organics equals unity, and the MGF_{org} including hygroscopic growth of organics

D_p (nm)	Mean			Differences (%)		
	DGF	MGF	MGF_{org}	$MGF-MGF_{org}$	DGF–MGF	$DGF-MGF_{org}$
80	1.45	1.4	1.42	1.4	3.4	2.1
140	1.53	1.43	1.47	2.8	6.5	3.9
250	1.6	1.48	1.49	0.7	7.5	6.9
380	1.56	1.57	1.59	1.3	0.6	1.9

Averages of all 12 h MOUDI-measurement time spans were made to derive the mean growth factors.

RH, respectively. The dew point mirror used to calibrate the humidity sensors of the H-DMPS has a systematic error of 0.5%. In sum, RHs had an uncertainty of 3.5% at 30–78% RH and 2% at 91% RH. Positive and negative variations of these magnitudes were made for the pre-defined RHs when determining the hygroscopic growth law (cf. Eq. (1)). For negative and positive RH variation, the percentage deviations of the DGF were +19% and −34%, respectively. Uncertainties of DGF are given at the 99% confidence level (three standard deviations).

Errors of the MGF arise due to uncertainties in the analytical methods and were estimated by varying the ion-mass concentration of each impactor stage by ±20% (uncertainty value given by E. Brüggemann, personal communication). Thereby, the estimated inorganic salt masses and the MGF on each impactor size range varied by about 25%.

3.5. Particle extinction coefficient σ_{ext}

Hygroscopic growth factors can be used to calculate the ambient PNSD and furthermore to estimate the optical particle properties at ambient RH with Mie calculations. The steps conducted to derive the particle extinction coefficient $\sigma_{ext,Mie}$ are presented in this section.

3.5.1. Determination of $\sigma_{ext,Mie}$

First, the PNSD at ambient RH for the 22 nm to 10 μm diameter range was derived by applying the extrapolated growth factors to the dry PNSD. Ambient RH in Xinken was measured with an automated meteorology monitoring station (cf. Fan et al., 2008). Then, the MOUDI stage-resolved complex refractive indices $\tilde{m}$ of particles were determined by using volume fractions of water ($\tilde{m} = 1.33 - 0i$), EC ($\tilde{m} = 1.8 - 0.54i$) and non-light-absorbing material ($\tilde{m} = 1.55 - 10^{-7}i$) present on each impactor size range. In the subsequent Mie calculations (Mie, 1908) to determine optical particle properties two different mixing-state models were used. In one model the aerosol particle population was assumed to consist of homogeneous, internally mixed particles interspersed with externally mixed EC. For these calculations, the derived mixing state of EC as presented by Cheng et al. (2006) was used. The homogeneously mixed particles in turn consist of three components: the internally mixed EC, the non-light-absorbing component and water. This model is referred to as Homogeneous Spheres Model (HSM). In the second model the assumption of coated particles with an elemental black carbon core and a shell consisting of an internal mix of non-light-absorbing material and water was made. This model is called Coated Spheres Model (CSM).

To simulate the uncertainties of the particle extinction coefficients, Monte Carlo simulations were performed as explained in Cheng et al. (2006). For that purpose several steps had to be carried out. At first, the uncertainties of the PNSD at ambient RH were simulated taking into account the uncertainties of the hygroscopic growth factors. Subsequently, the derived ambient PNSD uncertainties as well as the uncertainties of dry PNSD and MOUDI data as calculated in Cheng et al. (2006) were used to simulate the uncertainties of $\sigma_{ext,Mie}$. It was found that the uncertainties given as double standard deviation at a confidence level of 95% were humidity-dependent. For ambient RHs smaller than 80%, they amounted to 15% while they increased to 20% for RHs of 80–92%. The uncertainties were applied as error bars in Fig. 6.

3.5.2. Lidar-derived $\sigma_{ext,Lidar}$

The modeled $\sigma_{ext,Mie}$ were compared to those observed with a portable lidar system (Ansmann et al., 2005). The Raman lidar observed profiles of volume extinction and backscatter coefficients ($\sigma_{ext,Lidar}$ and β_{Lidar}) of ambient particles at 532 nm wavelength. Backscatter coefficients during night were determined down to 60 m height with the Raman method (Ansmann et al., 1992). To estimate the extinction coefficient $\sigma_{ext,Lidar}$ at this altitude, β_{Lidar} was multiplied with a height-averaged lidar ratio. Averaging was conducted over the lowest few hundred meters. As mentioned in Ansmann et al. (2005), the extinction coefficients could not be determined at 60 m during the day. Instead, they were calculated with an assumed constant lidar ratio (45 sr) and β_{Lidar} at 150–300 m. The resulting error of $\sigma_{ext,Lidar}$ is 30%.

4. Results and discussion

4.1. Growth factor dependence on local wind pattern

Chemical composition of the aerosol particles is different for different air masses. To investigate this dependence in more detail, hygroscopic growth factors were classified according to the wind direction near ground. DGF were measured for 20

days with a time resolution of 15 min. Growth factors derived from the impactor measurements had a time resolution of 12 h during 7 days measurement time. Therefore, a growth factor classification with respect to wind direction was made for the H-DMPS-derived DGF only. The time series of DGF at pre-defined RH of 30%, 57%, 78% and 91% were divided into three groups corresponding to times with prevailing surface wind directions of south–southeast (S–SE), north–northeast (N–NE) and calm conditions. Trajectories (calculated with the NOAA-Hysplit Model) indicated that air parcels in 500 and 1000 m height originated in the N–NE during the entire field campaign. As mentioned in Fan et al. (2008), influences of land–sea–breeze circulations on surface wind direction were observed when the region was dominated by a high pressure system with low wind speeds.

As shown in Fig. 4 and Table 3, DGF increased with increasing particle sizes until reaching a maximum in the accumulation range at about 250–300 nm. Size-dependent DGFs are a result of different amounts of soluble and insoluble material at different particles sizes. During N–NE winds, the transport of pollutants from urban and industrial regions to the field site was favored, resulting in lowest DGF. These values are about 15–35% lower than the average DGF observed at 91% RH. Higher than average DGF prevailed during times with calm wind or wind coming from the S–SE, i.e., the South Chinese Sea. Highest DGF were observed during calm wind conditions with values of 1.38, 1.62 and 1.68 at 50, 150 and 250 nm, respectively, being 12–15% above the average.

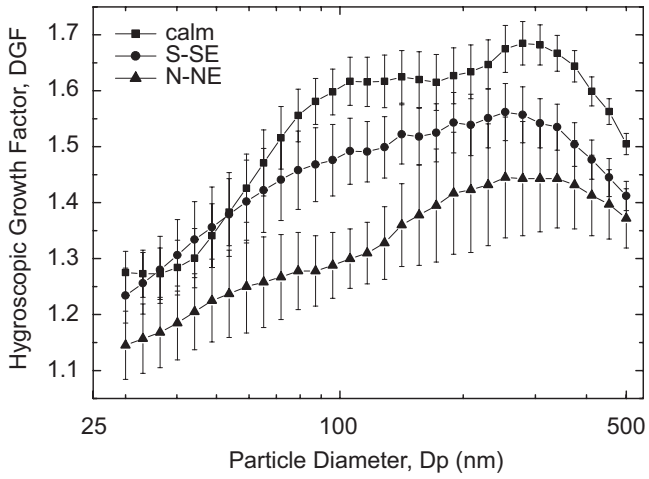

Fig. 4. DGF dependence on local wind patterns. Black squares refers to calm conditions, circles to winds from the S–SE, triangles to winds from the N–NE. Means and standard deviations are presented.

Table 3
DGF dependence on wind direction

Wind	$D_p = 50$ nm	$D_p = 150$ nm	$D_p = 250$ nm
Calm	1.38 ± 0.06	1.62 ± 0.05	1.68 ± 0.04
S–SE	1.38 ± 0.08	1.52 ± 0.05	1.56 ± 0.05
N–NE	1.24 ± 0.08	1.38 ± 0.09	1.45 ± 0.11
Mean	1.33 ± 0.07	1.48 ± 0.07	1.56 ± 0.07

Means and standard deviations are given for the DGF observed at three particle sizes at 91% relative humidity. The last row displays averages over all three groups.

In the left panels of Fig. 5 the PNSD at 78% and 91% RH as well the corresponding dry PNSD are shown. In the right panels, the wind direction-dependent DGF of all four pre-defined RH (30%, 57%, 78% and 91%) are presented. DGF strongly depend on the soluble mass fraction, which is the sum of the ion-mass concentrations divided by the dry total mass. During N–NE winds, a bimodal behavior of the DGF at 91% RH is obvious with a secondary maximum at about 60–70 nm (soluble mass fraction = 34%) and a primary maximum at 250–300 nm (soluble mass fraction = 49%). The soluble mass fraction in the size range between these maxima decreases to 29% resulting in a local minimum of DGF at 100 nm.

Fig. 5 shows a pronounced bimodal PNSD at 78% RH during the S–SE wind period. At 91% RH the PNSD has a broad maximum at 150–200 nm. The shape differences between the PNSD observed at 78% RH and 91% RH is probably caused by the different times at which the PNSD were measured. Shape differences can also be found in the DGF graphs. At 78% RH the curve is bimodal while at 91% RH it is smooth and monomodal.

The DGF at 91% RH during calm conditions shows a special feature. At about 40 nm a sudden increase in DGF is obvious. The strong gradient can be explained by an increase of the soluble mass fraction from 19% to 43% at corresponding particle sizes. The maximum DGF is reached at 250–300 nm. The strong hygroscopic growth with maximum DGF values of 1.68 at 250 nm cannot fully be explained by the soluble mass fraction of 48%. Instead, the high mass fraction of POM (24%) is thought to be at least partly hygroscopically active contributing to such high DGF.

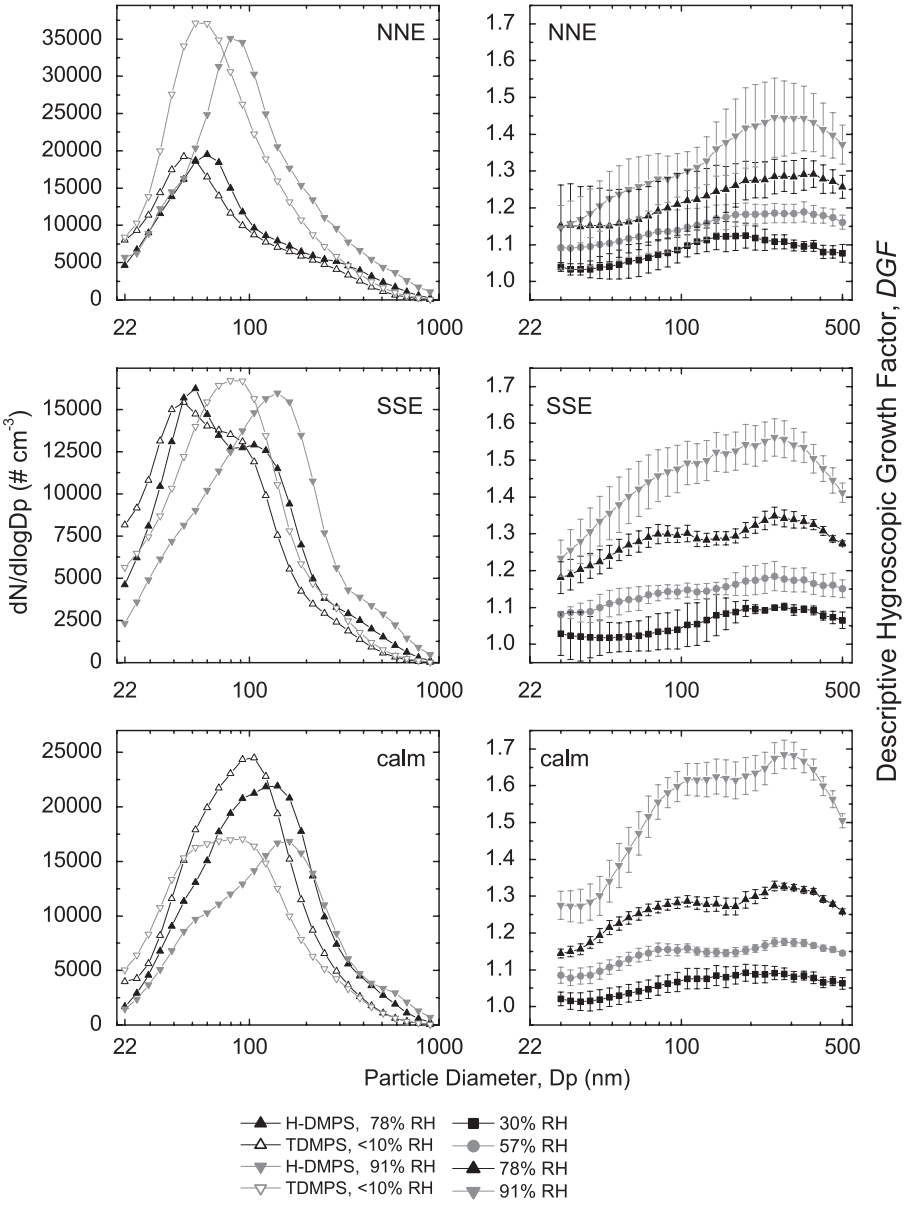

Fig. 5. Mean PNSD and DGF observed during different wind conditions. The upper panels refer to N–NE wind, i.e., wind coming from the Chinese mainland, the middle ones to S–SE wind, i.e., wind coming from the South Chinese Sea, and the lower ones to calm wind conditions. TDMPS-PNSD during which the H-DMPS was measuring at 78% RH and 91% RH are included in panels on the left side.

Additionally, the dependence of the DGF on time of day was investigated. During daytime (8.00–20.00) DGF were significantly higher (20–30%) than during nighttime (20.00–8.00). The difference is attributed to the boundary layer development. During the day, the planetary boundary layer (PBL) increased leading to a dilution of pollution by vertical mixing. After sunset, the PBL decrease was accompanied by a peak of biomass burning for cooking and diesel ships going upstream the Pearl River. The thereby emitted hydrophobic pollutants were trapped close to the ground resulting in lower DGF. Mean daytime soluble mass fractions of the considered size range exceeded the ones of the night measurements by about 14%.

4.2. Comparison of σ_{ext}

Particle extinction coefficients retrieved from Mie modeling with the HSM and CSM agreed very well, with differences of less than 3% (cf. Fig. 6). As mentioned in Section 3.5, a comparison between modeled $\sigma_{ext,Mie}$ and lidar-derived ones ($\sigma_{ext,Lidar}$) was made. Lidar data that had been averaged over

1 h during daytime and 2 h during nighttime was available. Mie-model results were also averaged over these time spans. In Fig. 6 time series of the measured and modeled extinction coefficients are shown for 23–26 October (DOY 297–300), the time period during which lidar and MOUDI measurements overlapped.

With mean values of 551 Mm^{-1}, $\sigma_{ext,Mie}$ determined with the HSM during 23–26 October is less than 1% higher than the mean $\sigma_{ext,Lidar}$ closest to the ground which amounts to 550 Mm^{-1}. $\sigma_{ext,Mie}$ derived from the CSM with an average of 537 Mm^{-1} is less than 3% lower than $\sigma_{ext,Lidar}$. Thereby it is shown that the outputs of both models agree well with the lidar-derived particle extinction coefficient $\sigma_{ext,Lidar}$.

This result is illustrated in Fig. 6 where trends of $\sigma_{ext,Mie}$ mostly agree with the $\sigma_{ext,Lidar}$ within their error bars. However, it should be emphasized that the displayed $\sigma_{ext,Lidar}$ was observed at 60 or 150–300 m height during night- or daytime, respectively, whereas the modeled extinction is based on surface measurements. Good agreement between $\sigma_{ext,Mie}$ and $\sigma_{ext,Lidar}$ can thus only be expected during times of a well-mixed boundary layer. Examples for such a well-mixed boundary layer during which deviations between the modeled and measured extinction coefficient were very small are 23 October 16.00–21.30 (DOY 297.67–297.95) and 24 October 14.00–19.00 (DOY 298.58–298.79). Days influenced by moderate to strong N–NE winds (25–26 October = DOY 299–300) also show good agreement between $\sigma_{ext,Lidar}$ and $\sigma_{ext,Mie}$ indicating well-mixed conditions in the lower part of the boundary layer.

On 24–25 October 23.00–1.00 (DOY 299.96–300.04) maximum deviations between $\sigma_{ext,Mie}$ and $\sigma_{ext,Lidar}$ were observed (cf. Fig. 6). Here, the modeled value was much higher than the lidar-derived one. This may be due to the pollution accumulation near the ground during that time which was also visible in the outputs of the nephelometer (TSI Model 3563) and the MAAP (Model Thermo 5012).

In Fig. 6, the humidity dependence of the particle extinction coefficient is also displayed. For that reason the dry particle extinction coefficient taken from Cheng et al. (2006) is shown. Dry σ_{ext} are based on measurements of the scattering coefficient and absorption coefficient of the nephelometer and the MAAP, respectively. As expected, differences between the dry and the ambient particle extinction coefficients are small when low ambient RHs were observed but increased with increasing RH. Fig. 6 illustrates the usefulness to model the extinction coefficient at ambient RH: Especially at high RHs

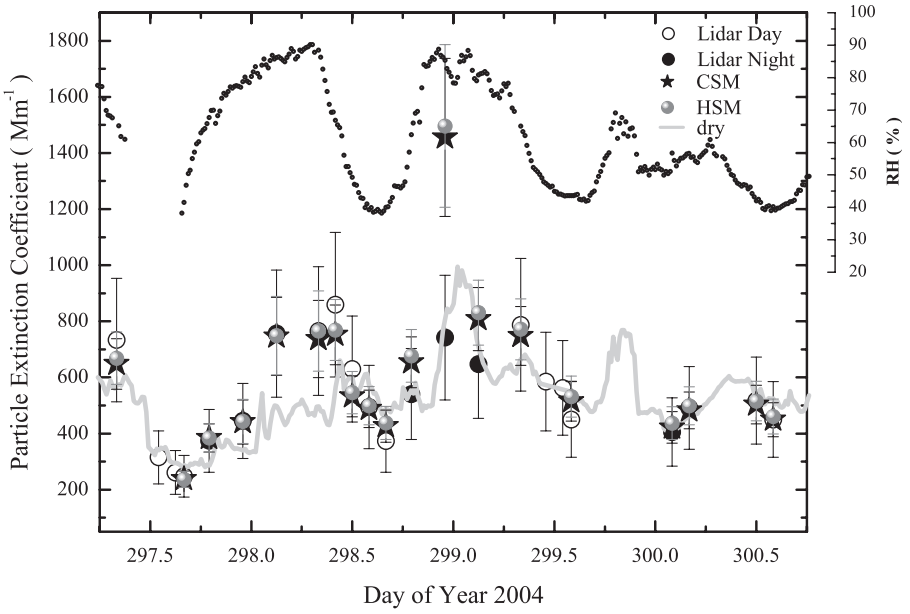

Fig. 6. Time series of modeled and lidar-derived particle extinction coefficients at 532 nm. CSM and HSM refer to the extinction coefficients calculated with the Coated Spheres Model and the Homogeneous Spheres Model, respectively. According to Section 4.2, error bars were applied. The gray line represents the dry particle extinction coefficient at 550 nm derived from measurements of the nephelometer and the MAAP as presented in Cheng et al. (2006). In addition, the relative humidity RH is shown.

as observed during DOY 298.0–298.3 the ambient extinction coefficient $\sigma_{ext,Mie}$ was able to reproduce the lidar-derived values while the dry extinction coefficient results were too low.

5. Summary and conclusions

Based on in situ aerosol microphysical and chemical measurements in fall 2004 at the rural background station Xinken in the highly polluted PRD region of China, hygroscopic growth factors of the aerosol particles were derived. An H-DMPS, was used to measure PNSD at pre-defined RH (30%, 57%, 78% and 91%). For the size range 30–500 nm descriptive hygroscopic growth factors (DGF) as functions of particle size were determined with the summation method by combining concurrent PNSD measurements of TDMPS and H-DMPS. DGFs observed in Xinken were size-dependent. Mean DGF observed at 91% relative humidity ranged from 1.2 to 1.57. Accumulation mode particles with a dry size of $D_p = 250$–300 nm exhibited the highest hygroscopic growth (mean DGF = 1.57). Aitken mode particles had significantly lower DGF. The most important factors influencing the observed DGF were the chemical composition which depended on wind direction and PBL development. Hygroscopic growth factors for the aerodynamic particle size range 0.1–5.6 μm were determined based on measurements of a 10-stage impactor operating at ambient relative humidity. The hygroscopic growth factors derived from two entirely different data sets and calculation methods were combined and extrapolated to derive hygroscopic growth properties to the entire size range 22 nm to 10 μm. A comparison between the hygroscopic growth factors derived from both methods showed agreement within the measurement uncertainties.

PNSDs at ambient RH were determined by applying the extrapolated size-resolved hygroscopic growth factors to the dry PNSD. By knowledge of this ambient PNSD, particle light extinction coefficients were derived from Mie calculations. For that purpose, two different mixing-state models were assumed. In the Coated Spheres Model (CSM), particles were assumed to consist of an EC core surrounded by a shell of non-light-absorbing material and water. In the Homogeneous Spheres Model (HSM), the particle population was treated as internally mixed spheres of EC, non-light-absorbing material and water interspersed with spheres of externally mixed EC.

Modeled σ_{ext} ranged from 180 to 1400 Mm^{-1} with mean values of about 550 ± 250 Mm^{-1}. These data were compared with the ones observed with the portable Raman lidar Polly. On average, the differences between the modeled and lidar-derived σ_{ext} were less than 3% which is smaller than the measurement uncertainties. It is concluded that measurements of PNSD (dry and humidified) in combination with size-resolved impactor measurements can be used to properly estimate the σ_{ext} at ambient relative humidity. The observed σ_{ext} are about 3–5 times higher than those observed in other campaigns conducted in Asian outflow regions (cf. Franke et al., 2003; Redemann et al., 2001), showing that the PRD is a highly polluted region.

Acknowledgments

This study was supported by the China National Basic Research and Development Programs 2002CB410801 and 2002CB211605.

References

Anderson, T.L., Charlson, R.J., Schwartz, S.E., Knutti, R., Boucher, O., Rodhe, H., Heintzenberg, J., 2003. Climate forcing by aerosols—a hazy picture. Science 300, 1103–1104.

Ansmann, A., Wandinger, U., Riebesell, M., Weitkamp, C., Michaelis, W., 1992. Independent measurements of extinction and backscatter profiles in cirrus clouds by using a combined Raman elastic-backscatter lidar. Applied Optics 31, 7113–7131.

Ansmann, A., Engelmann, R., Althausen, D., Wandinger, U., 2005. High aerosol load over the Pearl River Delta, China, observed with Raman lidar and Sun photometer. Geophysical Research Letters 32, L13815.

Birmili, W., Wiedensohler, A., 1997. The design of a twin differential mobility particle sizer for a wide size range and great operation stability. Journal of Aerosol Science 28, 145–146.

Birmili, W., Nowak, A., Schwirn, K., Lehmann, K., Massling, A., Wiedensohler, A., 2004. A new method to accurately relate dry and humidified number size distributions of atmospheric aerosols. Journal of Aerosol Science 1, 15–16 Abstracts of EAC, Budapest 2004.

Birmili, W., Schwirn, K., Nowak, A., Petäjä, T., Rose, D., Hämeri, K., Aalto, P., Joutsensaari, J., Wiedensohler, A., Kulmala, M., Boy, M., 2008. Hygroscopic growth of atmospheric particle number size distributions in the Finnish boreal forest region. Boreal Environmental Research, in submission.

Chan, M.N., Chan, C.K., 2005. Mass transfer effects in hygroscopic measurements of aerosol particles. Atmospheric Chemistry and Physics 5, 2703–2712.

Cheng, Y.F., Eichler, H., Wiedensohler, A., Heintzenberg, J., Zhang, Y.H., Hu, M., Herrmann, H., Zeng, L.M., Liu, S., Gnauk, T., Brüggemann, E., He, L.Y., 2006. The mixing state

of black carbon and non-light-absorbing aerosol components derived from in situ particle optical properties at Xinken in Pearl River Delta of China. Journal of Geophysical Research 111, D20204.

Cheng, Y.F., Wiedensohler, A., Eichler, H., Su, H., Gnauk, T., Brüggemann, E., Herrmann, H., Heintzenberg, J., Slanina, J., Tuch, T., Hu, M., Zhang, Y.H., 2008. Aerosol optical properties and related chemical apportionment at Xinken in Pearl River Delta of China. Atmospheric Environment, in this issue, doi:10.1016/j.atmosenv.2008.02.034.

Chuang, P.Y., 2003. Measurement of the timescale of hygroscopic growth for atmospheric aerosols. Journal of Geophysical Research 108, 4282.

Covert, D.S., Charlson, R.J., Ahlquist, N.C., 1972. A study of the relationship of chemical composition and humidity to light scattering by aerosols. Journal of Applied Meteorology 11, 968–976.

Dinar, E., Taraniuk, I., Graber, E.R., Anttila, T., Mentel, T.F., Rudich, Y., 2007. Hygroscopic growth of atmospheric and model humic-like substances. Journal of Geophysical Research 112, D05211.

Fan, S., Wang, B., Tesche, M., Engelmann, R., Althausen, A., Liu, J., Zhu, W., Fan, Q., Li, M., Ta, N., Song, L., Leong, K., 2008. Meteorological conditions and structures of atmospheric boundary layer in October 2004 over Pearl River Delta area. Atmospheric Environment, in this issue, doi:10.1016/j.atmosenv.2008.01.067.

Franke, K., Ansmann, A., Müller, D., Althausen, D., Venkataraman, C., Reddy, M., Wagner, F., Scheele, R., 2003. Optical properties of the Indo-Asian haze layer over the tropical Indian Ocean. Journal of Geophysical Research 108 (D2).

Gnauk, T., Müller, K., van Pinxteren, D., He, L.Y., Niu, Y.W., Hu, M., Herrmann, H., 2008. Size-segregated particulate chemical composition in Xinken, Pearl River Delta, China: OC/EC and organic compounds. Atmospheric Environment, this issue, doi:10.1016/j.atmosenv.2008.05.001.

Hänel, G., 1976. The properties of atmospheric aerosol particles as functions of the relative humidity at thermodynamic equilibrium with the surrounding moist air. Advances in Geophysics 19, 73–188.

Heintzenberg, J., Covert, D., 1990. On the distribution of physical and chemical particle properties in the atmospheric aerosol. Journal of Atmospheric Chemistry 10, 383–397.

IPCC2007: Forster, P., Ramaswamy, V., Artaxo, P., Berntsen, T., Betts, R., Fahey, D.W., Haywood, J., Lean, J., Lowe, D.C., Myhre, G., Nganga, J., Prinn, R., Raga, G., Schulz, M., Van Dorland, R., 2007. Changes in atmospheric constituents and in radiative forcing. In: Climate Change 2007: The Physical Science Basis. Contribution of Working Group I to the Fourth Assessment Report of the Intergovernmental Panel on Climate Change. Cambridge University Press, Cambridge, UK, New York, NY, USA.

Johnson, G., Ristovski, Z., Morawska, L., 2004. Method for measuring the hygroscopic behaviour of lower volatility fractions in an internally mixed aerosol. Journal of Aerosol Science 35, 443–455.

Kanakidou, M., Seinfeld, J.H., Pandis, S.N., Barnes, I., Dentener, F.J., Facchini, M.C., Van Dingenen, R., Ervens, B., Nenes, A., Nielsen, C.J., Swietlicki, E., Putaud, J.P., Balkanski, Y., Fuzzi, S., Horth, J., Moortgat, G.K., Winterhalter, R., Myhre, C.E.L., Tsigaridis, K., Vignati, E., Stephanou, E.G., Wilson, J., 2005. Organic aerosol and global climate modelling: a review. Atmospheric Chemistry and Physics 5, 1053–1123.

Liu, S., Hu, M., Slanina, J., He, L.Y., Niu, Y.W., Brüggemann, E., Gnauk, T., Herrmann, H., 2008. Size distribution and source analysis of ionic compositions of aerosols in polluted periods at Xinken in Pearl River Delta (PRD) of China. Atmospheric Environment, in this issue, doi:10.1016/j.atmosenv.2007.12.035.

Mader, B.T., Yu, J.Z., Xu, J.H., Li, Q.F., Wu, W.S., Flagan, R.C., Seinfeld, J.H., 2004. Molecular composition of the water-soluble fraction of atmospheric carbonaceous aerosols collected during ACE-Asia. Journal of Geophysical Research 109, D06206.

Mie, G., 1908. Beiträge zur Optik trüber Medien, speziell kolloidaler Metallösungen. Annals of Physics 25, 377–445.

Nowak, A., 2005. Das feuchte Partikelgrößenspektrometer: Eine neue Messmethode zur Bestimmung von Partikelgrößenverteilungen ($<1\,\mu m$) und größenaufgelösten hygroskopischen Wachstumsfaktoren bei definierten Luftfeuchten (The Humidifying Differential Mobility Particle Sizer: a new instrument to determine humidified particle number size distributions below $<1\mu m$ and size-resolved hygroscopic growth factors at defined relative humidities). Ph.D. Thesis, available at the Institute for Tropospheric Research (IfT) and the University of Leipzig.

Peng, C., Chan, M.N., Chan, C.K., 2001. The hygroscopic properties of dicarboxylic and multifunctional acids: measurements and UNIFAC predictions. Environmental Science and Technology 35, 4495–4501.

Redemann, J., Masonis, S., Schmid, B., Anderson, T., Russel, P., Livingston, J., Dubovik, O., Clarke, A., 2001. Clear-column closure studies of aerosols and water vapor aboard the NCAR C-130 during ACE-Asia. Journal of Geophysical Research 108 (D23).

Saxena, P., Hildemann, L., 1996. Water-soluble organics in atmospheric aerosol particles: a critical review of the literature and application of thermodynamics to identify candidate compounds. Journal of Atmospheric Chemistry 24, 57–109.

Sjogren, S., Gysel, M., Weingartner, E., Baltensperger, U., Cubison, M.J., Coe, H., Zardini, A.A., Marcolli, C., Krieger, U.K., Peter, T., 2007. Hygroscopic growth and water uptake kinetics of two-phase aerosol particles consisting of ammonium sulfate, adipic and humic acid mixtures. Journal of Aerosol Science 38, 157–171.

Stratmann, F., Wiedensohler, A., 1996. A new data inversion algorithm for DMPS measurements. Journal of Aerosol Science 27, 339–340.

Tang, I., 1981. The relative importance of atmospheric sulfates and nitrates in visibility reduction. Atmospheric Environment 15, 2463–2471.

Tang, I., 1996. Chemical and size effects of hygroscopic aerosols on light scattering coefficients. Journal of Geophysical Research 101, 19245–19250.

Tang, I., Munkelwitz, H., 1994. Water activities, densities, and refractive indices of aqueous sulfates and sodium nitrate droplets of atmospheric importance. Journal of Geophysical Research 99, 18801–18808.

Willeke, K., Baron, P.A. (Eds.), 1993. Aerosol Measurement: Principle, Techniques, and Applications. Van Nostrand Reinhold, New York.

Winkelmayr, P., 1991. A new electromobility spectrometer for the measurement of aerosol size distributions in the size

range from 1 to 1000 nm. Journal of Aerosol Science 22, 289–296.

Winkler, P., 1988. The growth of atmospheric aerosol particles with relative humidity. Physica Scripta 37, 223–230.

Zardini, A.A., Sjogren, S., Marcolli, C., Gysel, M., Weingartner, E., Baltensperger, U., Peter, T., 2008. A combined particle trap/HTDMA hygroscopicity study of mixed inorganic/organic aerosol particles. Atmospheric Chemistry and Physics Discussions 8, 5235–5268.

Zhang, Y.H., Hu, M., Zhong, L.J., Wiedensohler, A., Liu, S.C., Andreae, M.O., Wang, W., Fan, S.J., 2008. Regional integrated experiments of air quality over Pearl River Delta 2004 (PRIDE-PRD2004): overview. Atmospheric Environment, in this issue, doi:10.1016/j.atmosenv.2008.03.025.